Large-N seismic node networks for monitoring seismicity and crustal stress-state at geothermal systems

T. Hudson[1], T. Ketttlety[1], J. Kendall[1], S. Shams[1], T. O'Toole[2], N. Tranter[2], J. Holmgren[3], S. Lapins[4], E. MacDonald[5], M. Pinto Ward[1], R. Colquhoun[1], C. Judd[6], A. Jupe[7]

1 University of Oxford; 2 STRYDE Ltd; 3 NORSAR; 4 University of Bristol; 5 University of Glasgow; 6 Eden Geothermal Ltd; 7 Altcom Ltd

Summary

Geothermal resources are set to play an ever more important role in supplying a sustainable source of energy for the green transition. Here, we present an example of how recent developments in seismic node technology can provide enhanced monitoring of subsurface seismicity and crustal stress-state during geothermal field development. We show results for a network of 450 nodes deployed at a geothermal site in Cornwall, UK, during a well stimulation. A catalogue of 241 earthquakes are detected using a waveform-migration based method. The earthquakes are relocated using double-difference methods and used to map fault structure. Moment magnitudes, stress-drops, fault radii and focal mechanisms are calculated for the catalogue, in order to infer the stress-state of the faults and how fluids interact with the faults. Finally, S-wave velocity anisotropy measurements are used to compare local fault stresses to the orientation of the prevailing, macroscopic crustal stress-state. We find that the significant increase in spatial sampling provided by recent developments in seismic node technology allow us to elucidate fluid-fault interactions in far more detail than would otherwise be possible. These findings show the potential of recent technology advances for monitoring geothermal systems going forward.

Large-N seismic node networks for monitoring seismicity and crustal stress-state at geothermal systems

Introduction

The demand for energy over the next few decades is set to increase, with a desire to reduce global CO2 emissions at the same time. Geothermal systems provide one resource that can contribute towards both these energy production goals. While the concept of geothermal energy production is simple, the practical management of these subsurface fluids can be complex and expensive. Mapping crustal stresses and fault structures are important for informing operators of where the geothermal fluids migrate and accumulate, derisking exploration. Similarly, monitoring induced seismicity is important for mitigating seismic hazard. Recent advances in seismic node technology now allow for the deployment of 100s to 1000s of receivers at a similar cost to 10s of conventional instruments. This enables a significant increase in the density of sampling of the seismic wavefield (Ourabah & Chatenay, 2022). Here, we investigate how novel seismic node technology can be used to improve passive seismic mapping and monitoring of geothermal systems.

In this study we present analysis of data from a deployment of 450 Stryde nodes at a geothermal prospect in Cornwall, UK. Data were collected over a period of ~25 days in November to December 2022, during a period of well stimulation. A map of the network geometry can be seen in Figure 1. The nodes recorded continuous seismic data at a sampling rate of 500 Hz. Stryde nodes are single-component instruments, utilising piezoelectric technology, measuring acceleration with an approximately constant instrument response over frequencies of interest (1-100 Hz). However, here we not only deployed single nodes vertically, but at some locations deployed nodes in a three-component configuration, as well as deploying multiple nodes in the same orientation at some sites in order to investigate how stacking might improve data quality. In addition to the nodes, 10 conventional broadband seismometers were also deployed with a similar network aperture.

We first present a catalogue of relocated microseismicity, including temporal behaviour, as well as clustering and principal component analysis (PCA) to map fault/fracture orientations. These fault orientations are compared to fault orientations derived from moment tensor inversion and S-wave source polarisation analysis. Furthermore, we use seismic moment to investigate stress release during failure and fault areas. Cumulatively, these results allow not only for monitoring the seismicity through time, but also understanding the local stress conditions within the vicinity of the injection site. These local stress conditions are compared to the surrounding crustal stress conditions using shear-wave velocity anisotropy, measured via shear-wave splitting. Comparison of fault strikes and horizontal stress state also elucidates whether fluids are preferentially present along faults with a particular orientation (Hudson et al., 2023a). Finally, we conclude by briefly summarising the benefits and limitations of using seismic nodes for mapping and monitoring seismicity at geothermal prospects.

Methods

We detect microseismicity using a waveform-based back-migration method (Hudson et al., 2019; Smith et al., 2020). This searches for a coalescence of energy from all receivers in both space and time, minimising false triggers caused by incoherent noise sources. We detect ~250 earthquakes (see Figure 1). Seismicity are then initially relocated using NonLinLoc (Lomax & Virieux, 2000) before refining locations using a double-difference relative relocation method (Trugman & Shearer, 2017), based on cross-correlation derived relative arrival times. The velocity model used is the British Geological Survey SW England layered model. Clusters of seismicity are identified using a clustering algorithm, with PCA analysis applied to obtain the orientation of corresponding fault planes (see Hudson et al. (2022) for details of the method). Moment tensor source mechanism inversions are performed for the entire earthquake catalogue. Due to the volume of data (~250 earthquakes, each observed on up to 450 channels), we have to automate the source inversion procedure. Since we only have a 1D estimate of crustal velocity structure at the study site, we perform a P-wave polarity source inversion, rather than a full-waveform inversion, using the Bayesian MTFit source inversion algorithm (Pugh & White, 2018). P-wave polarities measured automatically (Pugh et al., 2016). Seismic moments are calculated by fitting a Brune model to the displacement spectra (Brune, 1970), with a spectral-ratio method used to isolate source and path effects (see Hudson et al. (2023b) for details). Seismic moments are still being

confirmed and so are not presented in this abstract. Isolating source and path effects allows us to measure crustal attenuation and earthquake corner frequencies more accurately, resulting in more accurate estimates of stress-drop and fault area. Source polarisations for each earthquake are calculated during shear-wave splitting analysis (see Hudson et al. (*in review*) for method), to account for crustal anisotropy effects on the measurements. Shear-wave fast directions are used to infer the orientation of the regional crustal stress state.

Seismicity

Figure 1 shows the microseismic catalogue detected by the node network. The seismicity are predominantly located within the immediate vicinity of the injection site, at depths of ~3.5 to 4 km bsl. Within the main cluster containing the majority of events, it is possible to somewhat discern two strikes, one ~90° from N (shallow, southerly cluster in Figure 1d) and another striking ~45° from N (deeper, northerly cluster, Figure 1d). Although we use a double-difference relocation method, hypocentral uncertainties are of the order of the inter-event spacing (10s to 100s metres). Analysis is also limited by a 1D velocity model.
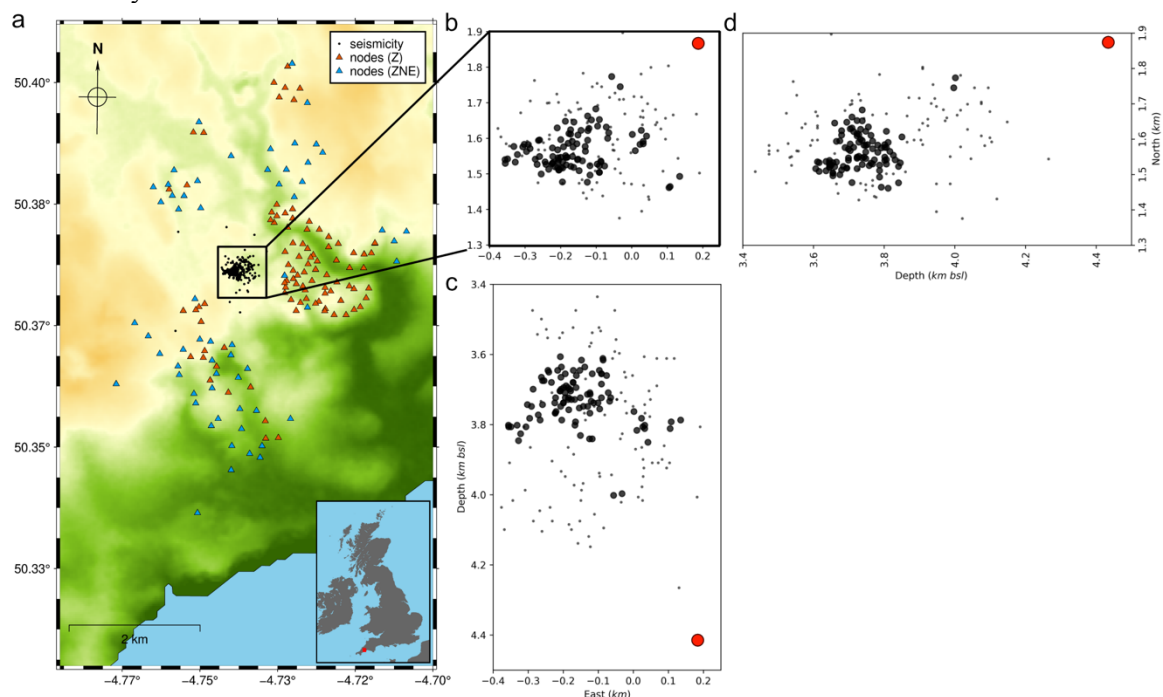

Figure 1 *Seismicity catalogue. a. Map of seismicity (black scatter points) and node receiver locations (orange triangles: single component sites; blue triangles: three-component sites). Larger black points are double-difference relocated. b-d. Detailed map and depth-section plots of the seismicity. Red point indicates earthquake corresponding to moment tensor in Figure 2.*

Subsurface stress-state

Earthquakes can provide various information to elucidate the subsurface stress state. A particularly useful observational constraint on subsurface stress are earthquake focal mechanisms, or moment tensor solutions. An example moment tensor from the most coherent earthquake in the dataset is shown in Figure 2. There is some uncertainty in the exact location of the nodal planes, as to be expected for polarity-based source inversions, especially when polarities are automatically estimated. Overall, the performance of the automatic polarity picker is remarkable, especially given that the data is derived from nodes, which are inevitably less sensitive than broadband instruments. The moment tensor suggests that the earthquake is a thrust-fault, with it more likely that the slip is sub-vertical ~10° from N, given that the overburden pressure is significantly greater than the lateral stress field.
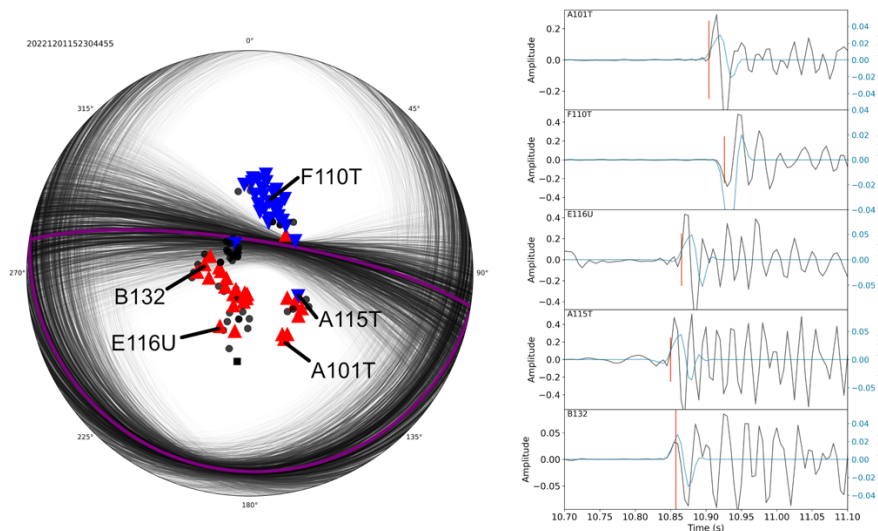
Figure 2 *Example moment tensor solution. Left: Lower hemisphere projection moment tensor solution. Scatter points indicate stations, coloured by polarity (red = compressional, blue = dilatational, black = undetermined). Purple line indicates most likely nodal planes, with black lines indicating a sample of the top 1% of possible solutions. Right: Examples of P-wave arrivals (black) with polarity probabilities (blue) and phase arrival times (red), for the five receivers labelled on the moment tensor solution.*

Figure 3 shows a comparison of the moment tensor slip direction to shear-wave splitting results for the entire dataset and regional stress orientations from the literature (Kingdon et al., 2022). Anisotropy-corrected S-wave source polarisations are generally consistent with the example moment tensor solution for the majority of events, suggesting consistent slip of earthquakes in the N-S axis. Anisotropic S-wave fast directions are dominantly oriented 20-30° from N. These represent anisotropy of the entire ray paths from the clusters of seismicity to the surface, and hence the bulk crustal anisotropy. One would expect the regional maximum horizontal stress to be oriented parallel to the dominant S-wave fast direction. However, that is not what we observe at the study site. We instead propose that the local maximum horizontal stress is instead oriented 20-30° from N based on the S-wave fast directions. This is consistent with the orientation of observed thrust faulting in Figure 2, with the earthquake strike 30° offset to the locally inferred max. horizontal stress, similar to the friction angle of the host rock (granite).
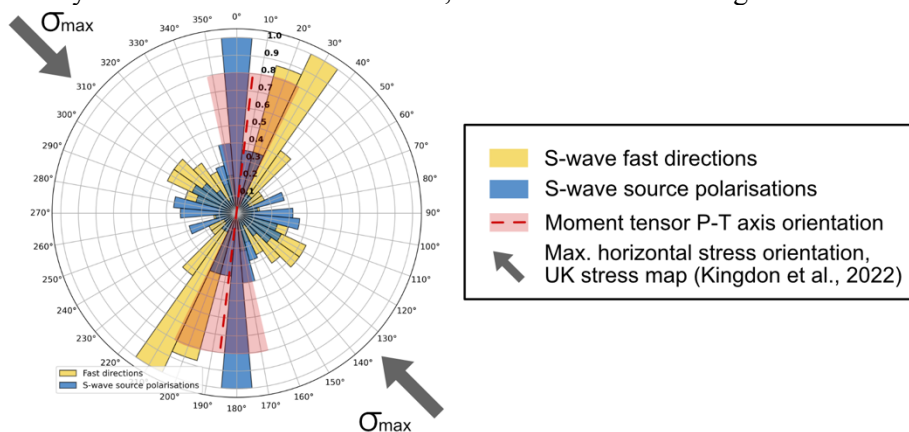

Figure 3 *Rose histogram summarising horizontal crustal and fault stress information. All orientations are in degrees from North. Normalised binned fast S-wave anisotropy directions for all event-receiver pairs are plotted in yellow and S-wave source polarisations in blue. P-T axis orientation for the example event moment tensor in Figure 2 are shown by the red dashed line, with red shading showing the corresponding uncertainty. Grey arrows indicate regional maximum horizontal stress direction ($\sigma_{h,max}$) from the UK stress map (Kingdon et al., 2022).*

Conclusions

A catalogue of ~250 earthquakes are detected at a geothermal system using 450 seismic nodes. Double difference relocation potentially indicates distinct clusters of seismicity, limited by hypocentral uncertainty. Automated polarity measurements constrain a moment tensor solution for an earthquake, showing a remarkably well constrained moment tensor given the automated nature of the input observations. The earthquake exhibits thrust faulting, assumed to slip sub-vertically, with the orientation consistent with the local maximum horizontal stress orientation inferred from S-wave anisotropy. Initial anisotropy-corrected S-wave source polarisations for the entire catalogue are also consistent with the example earthquake moment tensor solution. Overall, our results show that although individual seismic nodes are less sensitive than broadband instruments, exploiting the vast increase in spatial sampling shows considerable potential for monitoring and analysis of the stress-state of geothermal systems.

Acknowledgements

References

Brune, J. N. [1970]. Tectonic Stress and the Spectra of Seismic Shear Waves from Earthquakes. *Journal of Geophysical Research*, *75*(26), 4997–5009.

Hudson, T. S., Kendall, J. M., Blundy, J. D., Pritchard, M. E., MacQueen, P., Wei, S. S., Gottsmann, J.H., Lapins, S.. [2023a]. Hydrothermal Fluids and Where to Find Them: Using Seismic Attenuation and Anisotropy to Map Fluids Beneath Uturuncu Volcano, Bolivia. *Geophysical Research Letters*, *50*(5), 1–16.

Hudson, T. S., Kufner, S. K., Brisbourne, A. M., Kendall, J. M., Smith, A. M., Alley, R. B., Arthern, R. J., Murray, T.. [2023b]. Highly variable friction and slip observed at Antarctic ice stream bed. *Nature Geoscience*.

Hudson, T. S., Kendall, J. M., Pritchard, M. E., Blundy, J. D., & Gottsmann, J. H. [2022]. From slab to surface: Earthquake evidence for fluid migration at Uturuncu volcano, Bolivia. *Earth and Planetary Science Letters*, *577*, 117268.

Hudson, T. S., Smith, J., Brisbourne, A. M., & White, R. S. [2019]. Automated detection of basal icequakes and discrimination from surface crevassing. *Annals of Glaciology*, *60*(79), 167–181.

Hudson, T. S., Asplet, J., & Walker, A. M. [*in review*]. Automated shear-wave splitting analysis for single- and multi- layer anisotropic media. *Seismica*.

Kingdon, A., Williams, J., Fellgett, M., Rettelbach, N., & Heidbach, O. (2022). Stress Map of Great Britain and Ireland 2022. *GFZ German Research Center for Geosciences*.

Lomax, A., & Virieux, J. [2000]. Probabilistic earthquake location in 3D and layered models. *Advances in Seismic Event Location, Volume 18 of the Series Modern Approaches in Geophysics*, 101–134.

Ourabah, A., & Chatenay, A. [2022]. Unlocking ultra-high-density seismic for CCUS applications by combining nimble nodes and agile source technologies. *The Leading Edge*, *41*(1), 27–33.

Pugh, D. J., & White, R. S. [2018]. MTfit: A Bayesian Approach to Seismic Moment Tensor Inversion. *Seismological Research Letters*, *XX*(Xx), 1–7. https://doi.org/10.1785/0220170273

Pugh, D. J., White, R. S., & Christie, P. A. F. [2016]. Automatic Bayesian polarity determination. *Geophysical Journal International*, *206*(1), 275–291.

Smith, J. D., White, R. S., Avouac, J.-P., & Bourne, S. [2020]. Probabilistic earthquake locations of induced seismicity in the Groningen region, the Netherlands. *Geophysical Journal International*, *222*(1), 507–516.

Trugman, D. T., & Shearer, P. M. [2017]. GrowClust: A Hierarchical clustering algorithm for relative earthquake relocation, with application to the Spanish Springs and Sheldon, Nevada, earthquake sequences. *Seismological Research Letters*, *88*(2), 379–391.